



Cite this: *RSC Adv.*, 2022, 12, 1149

# Large improvement in thermoelectric performance of pressure-tuned $\text{Mg}_3\text{Sb}_2$ †

Juan Li, \* Shuai Zhang, Kai Han, Bing Sun and Lianzhen Cao

The  $\text{Mg}_3\text{Sb}_2$ -based Zintl compound is a promising candidate for a high-performance thermoelectric material with the advantage of the component elements being low cost, non-toxic and earth-abundant. Here, we investigate the influence of pressure on the electronic structure and p-type and n-type thermoelectric transport properties of  $\text{Mg}_3\text{Sb}_2$  by using density functional theory and Boltzmann transport theory. The energy gaps first increase and then decrease with the increasing of pressure, and a peak value of the valley degeneracy of conduction band occurs at 4 GPa. Based on the calculated band structures, the  $zT$  (figure of merit) values of p-type  $\text{Mg}_3\text{Sb}_2$  under pressure are significantly enhanced, which predominantly originates from the boosted PF (power factor) contributed by the increased carrier's relaxation time. When the carrier concentration reaches  $1 \times 10^{20} \text{ cm}^{-3}$ , the PF of p-type  $\text{Mg}_3\text{Sb}_2$  at 4 GPa is increased by 35% relative to that of the compound at 0 GPa, thus leading to a considerably improved  $zT$  of  $\sim 0.62$  at 725 K. Under the same conditions, due to the increased density of states effective mass, the n-type  $\text{Mg}_3\text{Sb}_2$  exhibits a highest PF of  $\sim 19 \mu\text{W cm}^{-1} \text{ K}^{-2}$  and a peak  $zT$  of 1.7. Therefore, pressure tuning is an effective method to improve the p-type and n-type thermoelectric transport performance of  $\text{Mg}_3\text{Sb}_2$ -based Zintl compounds. This work on  $\text{Mg}_3\text{Sb}_2$  under pressure may provide a new mechanism for the experimenters towards the enhancement of the thermoelectric performance of materials.

Received 8th December 2021  
Accepted 23rd December 2021

DOI: 10.1039/d1ra08930g

rsc.li/rsc-advances

## 1. Introduction

More than half the energy content of the fuel is lost as waste heat. Thermoelectrics is an effective technology of directly interconverting heat and electrical energy without moving parts, which can be applied in power generation and solid-state refrigeration.<sup>1–5</sup> Improving the energy conversion efficiency is the key factor influencing the extensive application of thermoelectric devices. The conversion efficiency is mainly governed by the performance of a thermoelectric material, which is quantified by the dimensionless figure of merit  $zT$ ,  $zT = S^2\sigma T/\kappa$ , where  $S$  is the Seebeck coefficient,  $\sigma$  is the electrical conductivity,  $\kappa$  is the thermal conductivity and  $T$  is the absolute temperature.<sup>6–8</sup> Therefore, increasing the power factor ( $S^2\sigma$ ) or decreasing the  $\kappa$  are significant ways to improve the  $zT$  and thereby to enhance the energy conversion efficiency of the thermoelectric devices.<sup>9–12</sup>

In addition to the thermoelectric material's performance, the cost and properties of the constituent elements also have an important influence on the widespread application of the thermoelectric technology. The advantage of the constituent

elements being low cost, non-toxic and earth-abundant make  $\text{Mg}_3\text{Sb}_2$ -based Zintl compounds promising candidates for high-performance thermoelectric materials.<sup>13–15</sup> By controlling the growing condition,  $\text{Mg}_3\text{Sb}_2$  can exhibit not only p-type transport performance but also n-type transport performance.<sup>16–21</sup> Pure  $\text{Mg}_3\text{Sb}_2$  is an intrinsic p-type semiconductor ascribed to the Mg vacancy responsible for the p-type carriers.<sup>19,20,22</sup> Song *et al.*<sup>23</sup> reported that through increasing the hole concentration, the  $zT$  value of 0.51 at 725 K can be achieved in p-type  $\text{Mg}_{2.985}\text{Ag}_{0.015}\text{Sb}_2$ . Due to the conduction band complexity,  $\text{Mg}_3\text{Sb}_2$  exhibits more outstanding n-type thermoelectric performance. Based on a defect chemistry approach, Tamaki *et al.*<sup>24</sup> reported n-type  $\text{Mg}_{3.2}\text{Sb}_{1.5}\text{Bi}_{0.49}\text{Te}_{0.01}$  with a high  $zT$  of 1.5 at 715 K, and similar results are reported by other groups.<sup>10,13,25–27</sup>

Pressure tuning<sup>28</sup> is an effective strategy for designing high-performance thermoelectric materials through modifying the electronic structure. Under pressure, the lattice parameters and band gaps of materials will be significantly changed, which will result in some positive changes in the electronic structures.<sup>29,30</sup> Because the key thermoelectric parameters ( $S$  and  $\sigma$ ) are strongly dependent on the electronic structure, therefore, the strategy based on pressure tuning can be used to improve the thermoelectric performance of materials. Zhang *et al.*<sup>31</sup> reported that the  $zT$  values of p-type SnSe along the  $b$  and  $c$  directions at 6 GPa and 700 K can be up to 2.5 and 1.7, respectively, and the  $zT$  of n-type sample at 600 K can reach 1.7. Polvani *et al.*<sup>32</sup>

Department of Physics and Optoelectronic Engineering, Weifang University, Weifang 261061, China. E-mail: lj\_wfu@163.com

† Electronic supplementary information (ESI) available. See DOI: 10.1039/d1ra08930g



reported that the  $zT$  value increased twofold in p-type  $\text{Sb}_{1.5}\text{Bi}_{0.5}\text{Te}_3$  upon pressure tuning. For improving the thermoelectric performance of  $\text{Mg}_3\text{Sb}_2$ , optimizing carrier concentration<sup>21,33–35</sup> or tuning carrier scattering mechanism<sup>10,26</sup> have been proved to be effective methods by a plenty of literatures, however, there are few theoretical reports about the method of pressure tuning. Therefore, it is necessary and important to investigate the effect of pressure on the thermoelectric properties of  $\text{Mg}_3\text{Sb}_2$ , which can provide significant guides for the experimental researchers.

The intention of this work is therefore to study the electronic structures and thermoelectric properties of  $\text{Mg}_3\text{Sb}_2$  at hydrostatic pressure by using first-principles calculations and Boltzmann transport theory. It is found that pressure tuning has a great influence on the band gap and valley degeneracy of  $\text{Mg}_3\text{Sb}_2$ . Due to the positive changes in the electronic structure, the p-type and n-type thermoelectric properties of  $\text{Mg}_3\text{Sb}_2$  are significantly improved. When the carrier concentration reaches  $1 \times 10^{20} \text{ cm}^{-3}$ , the  $zT$  of p-type  $\text{Mg}_3\text{Sb}_2$  at 4 GPa and 725 K can be up to  $\sim 0.62$ ,  $\sim 22\%$  higher than the value of the sample at 0 GPa, which predominantly originates from the considerably enhanced PF contributed by the increased carrier's relaxation

time. At the same temperature and carrier concentration, the n-type  $\text{Mg}_3\text{Sb}_2$  at 4 GPa can exhibit a high PF of  $\sim 19 \mu\text{W cm}^{-1} \text{ K}^{-2}$  and a peak  $zT$  of 1.7, which is mainly due to the increased density of states effective mass. These results demonstrate that pressure tuning is an effective way to the enhancement of the p-type and n-type thermoelectric transport properties of  $\text{Mg}_3\text{Sb}_2$ -based Zintl compounds.

## 2. Computation methods

In this work, the density functional theory (DFT) combined with the projector augmented wave (PAW) method are carried out to calculate the electronic structures of  $\text{Mg}_3\text{Sb}_2$  under different pressure, as implemented in the Vienna *Ab initio* Simulation Package (VASP).<sup>36–38</sup> The optimized crystal parameters of  $\text{Mg}_3\text{Sb}_2$  at 0 GPa can be obtained from our previous work.<sup>39,40</sup> Under the pressure ranging from 1 to 10 GPa, the structural relaxation including the lattice constants and internal coordinates are allowed to relax into their equilibrium positions. The modified Becke Johnson functional of the Tran and Blaha (TB-mBJ) potential<sup>41,42</sup> is adopted for obtaining the accurate electronic band structure. A  $12 \times 12 \times 8$  Monkhorst-Pack  $k$  mesh,

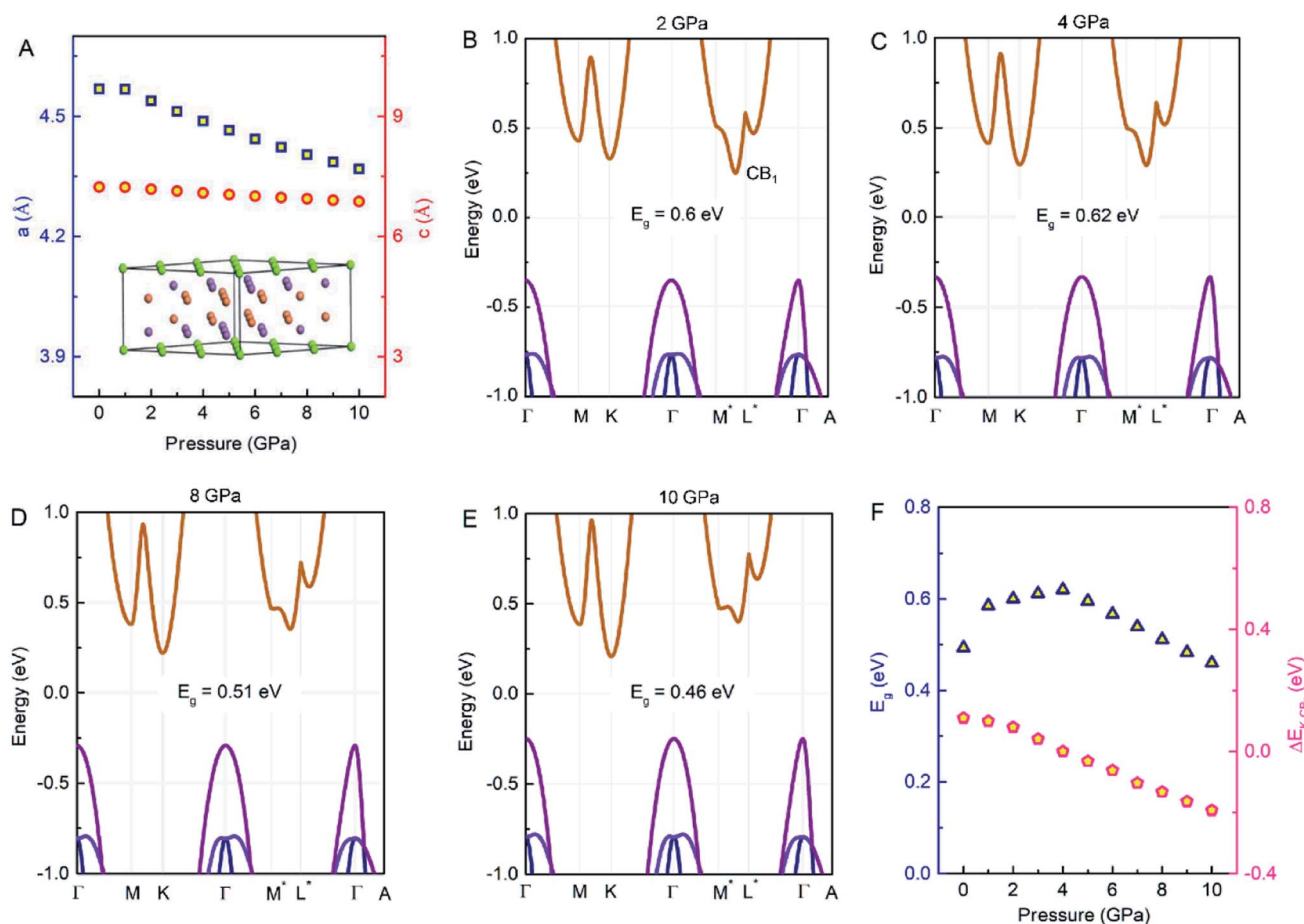


**Fig. 1** (A) Lattice parameters  $a$  and  $c$  as a function of the pressure. The insert panel is the crystal structure of  $\text{Mg}_3\text{Sb}_2$ , and the green, orange and purple balls represent Mg1, Mg2 and Sb atoms, respectively. (B–E) Calculated band structures of  $\text{Mg}_3\text{Sb}_2$  with pressure being 2, 4, 8 and 10 (unit: GPa). (F) The energy gap  $E_g$  and the energy difference  $\Delta E_{K-CB_1}$  between the  $K$  point in the band and  $CB_1$  band point as a function of pressure.



a plane-wave cutoff energy of 400 eV and an energy convergence criterion of  $10^{-4}$  eV are employed. Based on the calculated band structure, Effective Mass Calculator (EMC) program<sup>43</sup> is applied to calculate the effective masses. Considering that the spin orbit coupling (SOC) has an influence on the valence band of  $\text{Mg}_3\text{Sb}_2$ ,<sup>40</sup> the calculated band structures with SOC are used for the following electronic transport calculations.

The semi-classic Boltzmann transport theory is applied to calculate the electronic transport properties based on the calculated band structure with SOC, as implemented in the BoltzTraP2 code.<sup>44</sup> The calculation results can directly present the temperature and carrier concentration dependence of  $S$  and  $\sigma/\tau$  (where  $\tau$  is the carrier's relaxation time). In order to obtain the  $\sigma$ , the deformation potential theory<sup>45</sup> is employed to calculate the  $\tau$  and carrier mobility ( $\mu$ ). The minimum lattice thermal conductivity are evaluated using the Cahill's expression.<sup>46</sup>

### 3. Results and discussion

The layered Zintl compound  $\text{Mg}_3\text{Sb}_2$  crystallizes in an inverse  $\alpha$ - $\text{La}_2\text{O}_3$ -type structure which belongs to the space group  $P\bar{3}m1$ , as displayed in Fig. 1A. This structure can be described as the cationic  $\text{Mg}^{2+}$  layers intercalated between the anionic  $[\text{Mg}_2\text{Sb}_2]^{2-}$  layers. The Mg atoms in the ionic  $\text{Mg}^{2+}$  layers and in the covalently bonded  $[\text{Mg}_2\text{Sb}_2]^{2-}$  layers are denoted as Mg1 and Mg2, respectively. The optimized lattice constants of

$\text{Mg}_3\text{Sb}_2$  at 0 GPa from our previous work<sup>39,40</sup> are  $a = 4.568$  Å and  $c = 7.229$  Å. Fig. 1A shows the pressure dependence of the lattice parameters of  $\text{Mg}_3\text{Sb}_2$ . In the pressure range of 0 to 10 GPa, the lattice parameters decrease as the pressure increases, and the decrease of  $a$  is larger than that of  $c$ . The changes of the lattice parameters may have a significant influence on the electronic structures, and further affect the thermoelectric properties of  $\text{Mg}_3\text{Sb}_2$ .

The calculated band structures of  $\text{Mg}_3\text{Sb}_2$  with pressure being 2, 4, 8 and 10 GPa are shown in Fig. 1B–E. With the pressure increasing, the valence band maximum at the  $\Gamma$  point move upward, and the conduction band minimum at the  $K$  point shift downward, whereas the conduction band minimum at the  $\text{CB}_1$  point along the  $\text{M}^*-\text{L}^*$  line show an upward shift. When the pressure is below 4 GPa, the conduction band minimum is located at the  $\text{CB}_1$  point, however, when the pressure continues to increase, the conduction band minimum is located at the  $K$  point. The energy gaps of  $\text{Mg}_3\text{Sb}_2$  at 2, 4, 8 and 10 GPa are estimated to be 0.6, 0.62, 0.51 and 0.46 eV, respectively. In order to accurately describe the influence of pressure on the band gaps, the pressure dependence of the band gaps of  $\text{Mg}_3\text{Sb}_2$  are shown in Fig. 1F. The band gaps present a first increase and then decrease trend with the increase of pressure. Changes in the band gaps may have an impact on the band effective mass. It is clearly that the pressure has a large effect on the conduction band energy difference  $\Delta E_{K-\text{CB}_1}$  between the  $K$

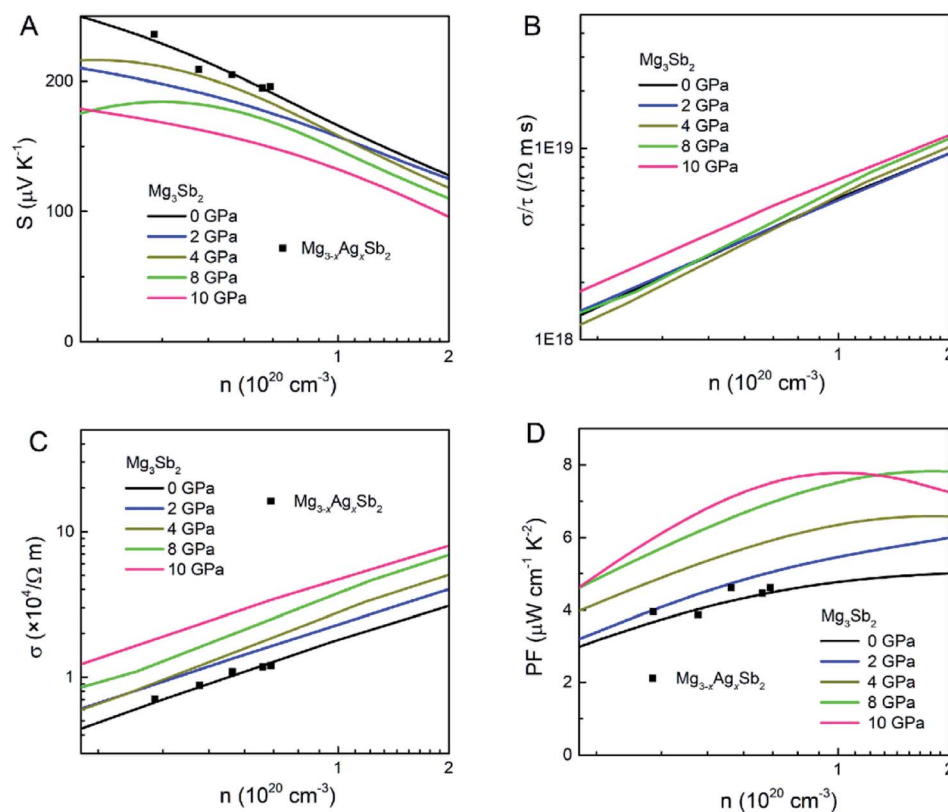


Fig. 2 The calculated (A) Seebeck coefficient  $S$ , (B) electrical conductivity with respect to relaxation time  $\sigma/\tau$ , (C) electrical conductivity  $\sigma$  and (D) power factor  $\text{PF}$  as a function of carrier concentration  $n$  for p-type  $\text{Mg}_3\text{Sb}_2$  at 725 K with pressure being 0, 2, 4, 8 and 10 (unit: GPa). The black squares are the experimental values of the reported  $\text{Mg}_{3-x}\text{Ag}_x\text{Sb}_2$  from ref. 23.

**Table 1** The calculated lattice elastic constant  $c_{11}$  (GPa), single valley effective mass  $m_s^*$  ( $m_e$ ) of the  $\Gamma$  valence band, conductivity effective mass  $m_i^*$  ( $m_e$ ) of the  $\Gamma$  valence band, the deformation potential  $\Xi$  (eV) of the valence band, and the carrier mobility  $\mu$  ( $\text{cm}^2 \text{V}^{-1} \text{s}^{-1}$ ) and relaxation time  $\tau$  (fs) at 725 K for p-type  $\text{Mg}_3\text{Sb}_2$  with pressure being 0, 2, 4, 8 and 10 (unit: GPa)

Pressure	$c_{11}$	$m_s^*$	$m_i^*$	$\Xi$	$\mu$	$\tau$
0	76.50 <sup>a</sup>	0.433	0.174	30.7	33.18	3.29
2	80.74	0.416	0.175	25.5	43.07	4.28
4	89.78	0.414	0.186	25.0	49.69	4.96
8	102.45	0.407	0.200	24.4	53.97	6.13
10	108.49	0.402	0.203	24.0	59.29	6.84

<sup>a</sup> Ref. 40.

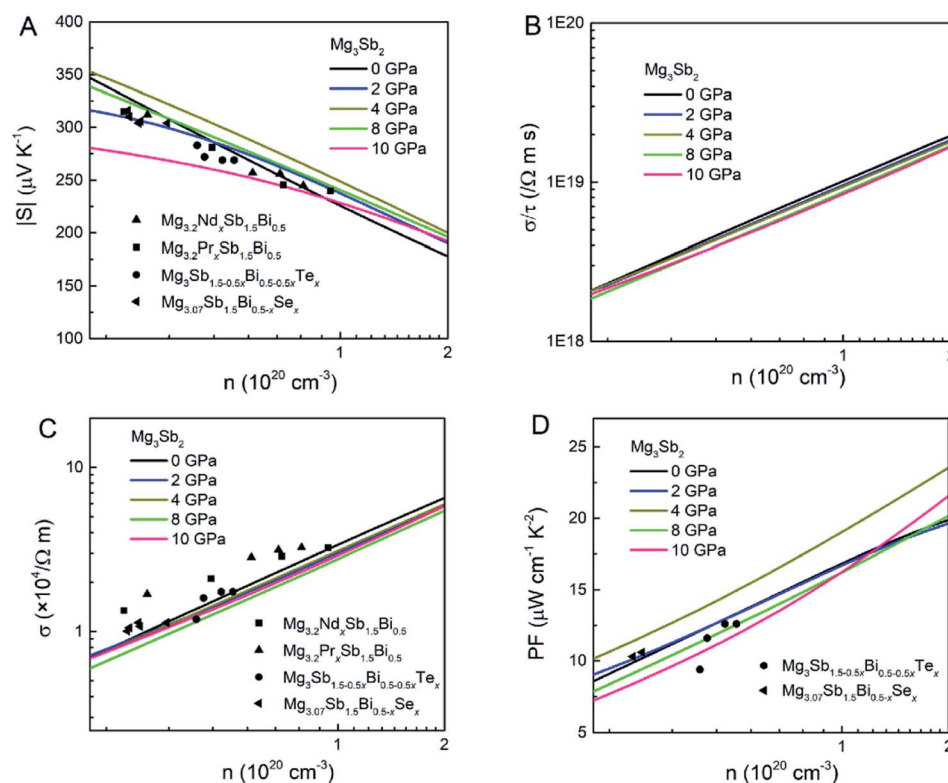
point in the band and  $\text{CB}_1$  band point. As can be seen from Fig. 1F, with the increase of pressure, the absolute value of  $\Delta E_{\text{K-CB}_1}$  decrease firstly and then increase. When the pressure increases to 4 GPa,  $\Delta E_{\text{K-CB}_1}$  approaches to nearly zero, giving rise to a peak in the valley degeneracy ( $N_v = 11$ ). Because the thermoelectric parameters are closely associated with the band effective mass and valley degeneracy, pressure tuning may be an effective way to achieve high-thermoelectric properties of  $\text{Mg}_3\text{Sb}_2$ -based materials.

Fig. 2 shows the  $S$ ,  $\sigma/\tau$ ,  $\sigma$  and PF as a function of carrier concentration for p-type  $\text{Mg}_3\text{Sb}_2$  at 725 K with pressure being 0,

2, 4, 8 and 10 GPa, and the comparison with the experimental data of the reported  $\text{Mg}_{3-x}\text{Ag}_x\text{Sb}_2$  sample. The calculated  $S$  consistent with the experimental value verifies the accuracy of our computation methods. The  $S$  of p-type  $\text{Mg}_3\text{Sb}_2$  under different pressure has a negative relationship with the carrier concentration in certain doping range. At the same carrier concentration, the  $S$  calculated at 2, 4, 8 and 10 GPa are smaller than the value calculated at 0 GPa, which indicates that pressure tuning has a detrimental influence on the  $S$  of p-type  $\text{Mg}_3\text{Sb}_2$ . In order to analyze the reason for the decrease of  $S$  under pressure, we calculate the single valley effective mass  $m_s^*$  of the  $\Gamma$  valence band based on the electronic band structure (see Table 1). The relationship between  $S$  and  $m_s^*$  is given by:<sup>47</sup>

$$S = \frac{2k_B^2 T}{3e(h/2\pi)^2} N_v^{2/3} m_s^* \left( \frac{\pi}{3n} \right)^{2/3} \quad (1)$$

where  $m_s^*$  is the single valley effective mass,  $N_v$  is the valley degeneracy,  $n$  is the carrier concentration,  $T$  is the absolute temperature,  $h$  is the Planck constant and  $k_B$  is the Boltzmann constant. According to the equation, the  $S$  is in positive correlation with the density of states effective mass ( $m_d^* = N_v^{2/3} m_s^*$ ). The  $m_s^*$  of the  $\Gamma$  valence band at 0, 2, 4, 8 and 10 GPa are estimated to be 0.433  $m_e$ , 0.416  $m_e$ , 0.414  $m_e$ , 0.407  $m_e$  and 0.402  $m_e$ , respectively, which reveals that pressure tuning may lead to a decrease in the  $m_s^*$  of the  $\Gamma$  valence band. Due to the negligible effect of the pressure on the valley degeneracy of the  $\Gamma$  valence band (Fig. 1B–E), the decreased  $S$  of p-type  $\text{Mg}_3\text{Sb}_2$  by pressure



**Fig. 3** The calculated (A) Seebeck coefficient  $S$ , (B) electrical conductivity with respect to relaxation time  $\sigma/\tau$ , (C) electrical conductivity  $\sigma$  and (D) power factor PF as a function of carrier concentration for n-type  $\text{Mg}_3\text{Sb}_2$  at 725 K with pressure being 0, 2, 4, 8 and 10 (unit: GPa). The experimental data of the n-type  $\text{Mg}_{3.2}\text{Nd}_x\text{Sb}_{1.5}\text{Bi}_{0.5}$ ,<sup>33</sup>  $\text{Mg}_{3.2}\text{Pr}_x\text{Sb}_{1.5}\text{Bi}_{0.5}$ ,<sup>25</sup>  $\text{Mg}_3\text{Sb}_{1.5-0.5x}\text{Bi}_{0.5-0.5x}\text{Te}_x$  (ref. 14) and  $\text{Mg}_{3.07}\text{Sb}_{1.5}\text{Bi}_{0.5-x}\text{Se}_x$  (ref. 13) samples are plotted for comparison.



tuning may be mainly ascribed to the decrease of the  $m_s^*$  of the  $\Gamma$  valence band.

As shown in Fig. 2B, the  $\sigma/\tau$  of p-type  $\text{Mg}_3\text{Sb}_2$  at 0, 2, 4, 8 and 10 GPa show an increasing trend as the carrier concentration increases. The  $\tau$  for determining the  $\sigma$  can be estimated by the deformation potential theory, as expressed as:<sup>40,48</sup>

$$\mu = \frac{2\sqrt{2}\pi e(h/2\pi)^4 c_{ii}}{3(k_B T)^{3/2} m_s^{*3/2} m_l^* \Xi^2} \quad (2)$$

$$\tau = \frac{\mu m_l^*}{e} = \frac{2\sqrt{2}\pi(h/2\pi)^4 c_{ii}}{3(k_B T m_s^*)^{3/2} \Xi^2} \quad (3)$$

where  $\mu$  is the carrier mobility,  $m_s^*$  is the single valley effective mass,  $m_l^*$  is the conductivity effective mass,  $\Xi$  is the deformation potential,  $c_{ii}$  is lattice elastic constant,  $h$  is the Planck constant and  $k_B$  is the Boltzmann constant. The larger the value of  $c_{ii}$  and the smaller the values of  $m_s^*$  and  $\Xi$ , the better the performance of  $\tau$ . Table 1 lists the input parameters and the calculated  $\tau$  at 725 K for p-type  $\text{Mg}_3\text{Sb}_2$  with pressure being 0, 2, 4, 8 and 10 GPa. With the increasing of pressure, the increased  $c_{11}$  and the decreased  $m_s^*$  and  $\Xi$  are beneficial to the  $\tau$ . The  $\tau$  at 0, 2, 4, 8 and 10 GPa are estimated to be 3.29, 4.28, 4.96, 6.13 and 6.84 fs, respectively. Based on the calculated  $\tau$ , the  $\sigma$  as a function of carrier concentration for p-type  $\text{Mg}_3\text{Sb}_2$  with pressure being 0, 2, 4, 8 and 10 GPa are plotted in Fig. 2C. At the same carrier concentration, because of the enhanced  $\tau$ , there is an improvement in the  $\sigma$  with the increase of pressure. As a result of the largely improved  $\sigma$ , the theoretical PF for p-type  $\text{Mg}_3\text{Sb}_2$  is strongly enhanced as the pressure increases (Fig. 2D). Because there may exist phase transition in  $\text{Mg}_3\text{Sb}_2$  at pressure above 5 GPa,<sup>49,50</sup> therefore, pressure tuning on p-type thermoelectric properties require careful selection of the pressure. When the carrier concentration increases up to  $1 \times 10^{20} \text{ cm}^{-3}$ , p-type  $\text{Mg}_3\text{Sb}_2$  at 4 GPa exhibits a high PF of  $\sim 6.2 \mu\text{W cm}^{-1} \text{ K}^{-2}$ , 35% higher than the value of  $\sim 4.6 \mu\text{W cm}^{-1} \text{ K}^{-2}$  for the compound at 0 GPa. Therefore, pressure tuning can make a significant contribution to the excellent p-type electronic transports for  $\text{Mg}_3\text{Sb}_2$ -based compounds.

Fig. 3 shows the  $S$ ,  $\sigma/\tau$ ,  $\sigma$  and PF as a function of carrier concentration for n-type  $\text{Mg}_3\text{Sb}_2$  at 725 K with pressure being 0, 2, 4, 8 and 10 GPa, and the comparison with the experimental data of the reported Nd-, Pr-, Te- and Se-doped  $\text{Mg}_3\text{Sb}_2$ -based compounds. The discrepancy between the simulated results and the experimental data is mainly ascribed to the effect of Bi doping on the electrical transport properties of  $\text{Mg}_3\text{Sb}_2$ .<sup>39</sup> At the same carrier concentration, compared to the samples at 0, 2, 8 and 10 GPa, the n-type  $\text{Mg}_3\text{Sb}_2$  at 4 GPa possesses a higher  $S$ . As can be seen from Table 2, with the increase of pressure, the  $m_s^*$  of the  $\text{CB}_1$  conduction band ( $m_{s, \text{CB}_1}^*$ ) increases, whereas the  $m_s^*$  of the K conduction band ( $m_{s, \text{K}}^*$ ) decreases. Because of the smaller absolute value of  $\Delta E_{\text{K-CB}_1}$  (below  $\sim 0.11 \text{ eV}$ ) at 0, 2 and 4 GPa (Fig. 1F), the average  $m_s^*$  (0.252  $m_e$ , 0.255  $m_e$  and 0.257  $m_e$ ) of the both bands are used for calculating the  $\tau$ . The increased  $m_s^*$  and the highest valley degeneracy (Fig. 2C) mainly contribute to the excellent  $S$  of n-type  $\text{Mg}_3\text{Sb}_2$  at 4 GPa.

**Table 2** Calculated single valley effective mass  $m_{s, \text{K}}^*$  ( $m_e$ ) of the K conduction band, single valley effective mass  $m_{s, \text{CB}_1}^*$  ( $m_e$ ) of the  $\text{CB}_1$  conduction band, conductivity effective mass  $m_{l, \text{K}}^*$  ( $m_e$ ) of the K conduction band, conductivity effective mass  $m_{l, \text{CB}_1}^*$  ( $m_e$ ) of the  $\text{CB}_1$  conduction band, the deformation potential  $\Xi$  (eV) of the conduction band, and the carrier mobility  $\mu$  ( $\text{cm}^2 \text{ V}^{-1} \text{ s}^{-1}$ ) and relaxation time  $\tau$  (fs) at 725 K for n-type  $\text{Mg}_3\text{Sb}_2$  with pressure being 2, 4, 8 and 10 (unit: GPa), in comparison with the previously reported values at 0 GPa

Pressure	$m_{s, \text{K}}^*$	$m_{s, \text{CB}_1}^*$	$m_{l, \text{K}}^*$	$m_{l, \text{CB}_1}^*$	$\Xi$	$\mu$	$\tau$
0	0.299 <sup>a</sup>	0.205 <sup>a</sup>	0.289 <sup>a</sup>	0.178 <sup>a</sup>	45.0 <sup>a</sup>	27.00 <sup>a</sup>	3.33 <sup>a</sup>
2	0.297	0.212	0.287	0.18	43.0	25.14	3.16
4	0.293	0.220	0.283	0.186	44.5	25.85	3.29
8	0.287	0.235	0.278	0.196	43.9	20.25	3.42
10	0.285	0.242	0.276	0.201	43.7	22.03	3.45

<sup>a</sup> Ref. 40.

As shown in Table 2, the calculated  $\tau$  for n-type  $\text{Mg}_3\text{Sb}_2$  at 2, 4, 8 and 10 GPa are 3.16, 3.29, 3.42 and 3.45 fs, respectively. It is clearly that there is no obvious improvement in  $\tau$  with the increasing of the pressure, which may be ascribed to the moderately changed  $\mu$  according to the equation  $\sigma = ne\mu$ .<sup>39</sup> Based on the calculated  $\tau$  using the deformation potential theory, the  $\sigma$  as a function of carrier concentration for n-type  $\text{Mg}_3\text{Sb}_2$  at 725 K with pressure being 0, 2, 4, 8 and 10 GPa are plotted in Fig. 3C. The  $\sigma$  shows an increasing trend as the pressure increases. Owing to the not remarkably increased  $\tau$ , the contribution of the pressure tuning to the  $\sigma$  is not significant. Combined the calculated  $S$  and  $\sigma$ , Fig. 3D presents the PF as a function of carrier concentration for n-type  $\text{Mg}_3\text{Sb}_2$  under different pressure. The synergistic effect of the increased  $S$  and the moderately changed  $\sigma$  at 4 GPa make the n-type  $\text{Mg}_3\text{Sb}_2$  possess the highest PF of  $\sim 19 \mu\text{W cm}^{-1} \text{ K}^{-2}$  at the carrier concentration of  $1 \times 10^{20} \text{ cm}^{-3}$ . Therefore, further optimization of the electronic transport properties in n-type  $\text{Mg}_3\text{Sb}_2$ -based materials can be expected through pressure tuning.

The  $\kappa$  is generally composed of the electronic thermal conductivity ( $\kappa_e$ ) and lattice thermal conductivity ( $\kappa_l$ ). The observed  $\kappa_l$  of  $\text{Mg}_3\text{Sb}_2$ -based materials in the experiments can reach the minimum lattice thermal conductivity ( $\kappa_{\text{min}}$ ).<sup>24,25,51</sup> In order to investigate the effect of the pressure on the thermal

**Table 3** The calculated bulk modulus  $B$  (GPa), shear modulus  $G$  (GPa), transversal velocity  $v_t$  ( $\text{m s}^{-1}$ ), longitudinal velocity  $v_l$  ( $\text{m s}^{-1}$ ), and the minimum lattice thermal conductivity  $\kappa_{\text{min}}$  ( $\text{W m}^{-1} \text{ K}^{-1}$ ) for  $\text{Mg}_3\text{Sb}_2$  with pressure being 2, 4, 8 and 10 (unit: GPa), in comparison with the previously reported values at 0 GPa

Pressure	$B$	$G$	$v_t$	$v_l$	$\kappa_{\text{min}}$
0	45.60 <sup>a</sup>	17.87 <sup>a</sup>	2107.68 <sup>a</sup>	4154.64 <sup>a</sup>	0.53 <sup>a</sup>
2	47.74	20.72	2247.47	4285.95	0.56
4	53.84	23.49	2350.34	4475.30	0.60
8	64.74	27.99	2491.03	4755.13	0.66
10	69.62	29.53	2526.50	4853.62	0.68

<sup>a</sup> Ref. 40.



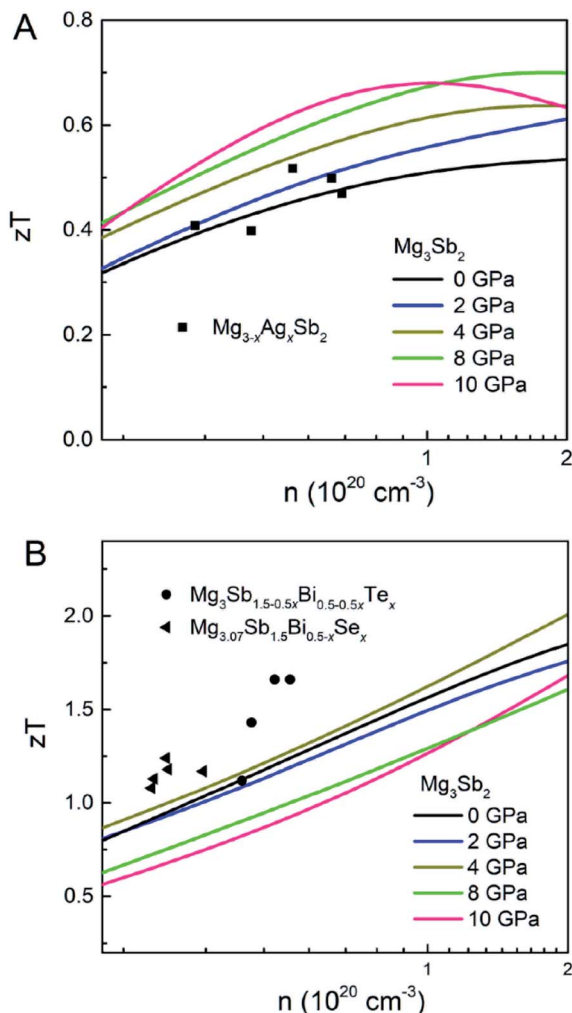


Fig. 4 The calculated  $zT$  as a function of carrier concentration for (A) p-type and (B) n-type  $\text{Mg}_3\text{Sb}_2$  at 725 K with pressure being 0, 2, 4, 8 and 10 (unit: GPa). In (A), the black squares represent the previously reported p-type  $\text{Mg}_{3-x}\text{Ag}_x\text{Sb}_2$ .<sup>23</sup> In (B), the black circles and triangles represent the previously reported n-type  $\text{Mg}_3\text{Sb}_{1.5-0.5x}\text{Bi}_{0.5-0.5x}\text{Te}_x$  and  $\text{Mg}_{3.07}\text{Sb}_{1.5}\text{Bi}_{0.5-x}\text{Se}_x$ .<sup>13,14</sup>

transport performance, the  $\kappa_{\min}$  for  $\text{Mg}_3\text{Sb}_2$  at different pressure are calculated using the Cahill's formula:<sup>39,40</sup>

$$\kappa_{\min} = \frac{1}{2} \left( \frac{\pi}{6} \right)^{1/3} k_B (V)^{-2/3} (2\nu_s + \nu_l) \quad (4)$$

$$\nu_l = \sqrt{\frac{G}{\rho}} \quad (5)$$

$$\nu_s = \sqrt{\left( B + \frac{4}{3}G \right) / \rho} \quad (6)$$

where the  $\nu_s$  and  $\nu_l$  represent the transverse and longitudinal speed of sound, respectively, and the  $B$  and  $G$  denote the bulk and shear modulus, respectively. The input parameters and the calculated  $\kappa_{\min}$  are displayed in Table 3. These key parameters ( $\nu_s$ ,  $\nu_l$ ,  $B$  and  $G$ ) increase with the increasing of the pressure, which is detrimental to the  $\kappa_{\min}$  of  $\text{Mg}_3\text{Sb}_2$ . The  $\kappa_{\min}$  at 2, 4, 8

and 10 GPa are estimated to be 0.56, 0.60, 0.66 and 0.68  $\text{W m}^{-1} \text{K}^{-1}$ , respectively, slightly higher than the value at 0 GPa (0.53  $\text{W m}^{-1} \text{K}^{-1}$ ). These results reveal that pressure tuning is not conducive to the reduction of the  $\kappa_{\min}$  of  $\text{Mg}_3\text{Sb}_2$ -based compounds.

The experimental  $\kappa_e$  for p-type and n-type  $\text{Mg}_3\text{Sb}_2$  at 725 K are in the range of 0.1–0.2  $\text{W m}^{-1} \text{K}^{-1}$  and 0.14–0.36  $\text{W m}^{-1} \text{K}^{-1}$ , respectively.<sup>23,25,33,34,52</sup> Here, the average  $\kappa_e$  (0.15  $\text{W m}^{-1} \text{K}^{-1}$  and 0.25  $\text{W m}^{-1} \text{K}^{-1}$  respectively for p-type and n-type sample) and the  $\kappa_{\min}$  are applied for estimating the  $\kappa$ . Based on the calculated PF and  $\kappa$ , Fig. 4 shows the simulated  $zT$  for p-type and n-type  $\text{Mg}_3\text{Sb}_2$  at 725 K with pressure being 0, 2, 4, 8 and 10 GPa, and the comparison with the previously reported experimental data. As can be seen from Fig. 4A, the calculated  $zT$  of p-type  $\text{Mg}_3\text{Sb}_2$  basically coincide with the experimental data, which demonstrates the correctness of the computational methods. It is found that the  $zT$  values of p-type  $\text{Mg}_3\text{Sb}_2$  at 2, 4, 8 and 10 GPa are significantly improved compared to the value of the sample at 0 GPa. The largely enhanced thermoelectric performance of the sample by the pressure predominantly originates from the considerably increased PF. As a result, when the carrier concentration reaches  $1 \times 10^{20} \text{ cm}^{-3}$ , the p-type  $\text{Mg}_3\text{Sb}_2$  at 4 GPa exhibits a peak  $zT$  of  $\sim 0.62$ ,  $\sim 22\%$  higher than the value of the sample at 0 GPa. Compared to the experimental data, the underestimated  $zT$  of n-type  $\text{Mg}_3\text{Sb}_2$  calculated by the DFT method can be ascribed to the neglect of the contribution of the Bi doping on the  $\kappa_1$  and PF.<sup>6,39</sup> (Fig. 4B). Among all samples, the  $\text{Mg}_3\text{Sb}_2$  at 4 GPa shows the best n-type performance with a  $zT$  of 1.7 at the carrier concentration of  $1 \times 10^{20} \text{ cm}^{-3}$ , which is mainly resulting from the increased PF. Based on the above analysis, a conclusion can be drawn that the pressure tuning is an effective method to achieve an enhancement of not only p-type but also n-type thermoelectric performance of  $\text{Mg}_3\text{Sb}_2$ -based Zintl compounds.

## 4. Conclusion

In this work, we have investigated the influence of the pressure on the electronic band structures and p-type and n-type thermoelectric transport properties of  $\text{Mg}_3\text{Sb}_2$  by using the density functional theory and semi-classic Boltzmann transport theory. According to the calculated results of the band structure, increasing pressure can lead the energy gaps to first increase and then decrease, and the pressure of 4 GPa can contribute to a peak value of the valley degeneracy of the conduction band. Because of the increased  $\tau$ , the PF of p-type  $\text{Mg}_3\text{Sb}_2$  at 4 GPa and 725 K is increased by  $\sim 35\%$  percent than that of the compound at 0 GPa, thus leading to a considerably enhanced  $zT$  of  $\sim 0.62$  at the carrier concentration of  $1 \times 10^{20} \text{ cm}^{-3}$ . Besides its impact on the p-type transports, pressure tuning can also influence the n-type transports of  $\text{Mg}_3\text{Sb}_2$ . When the pressure increases up to 4 GPa, the n-type sample at the carrier concentration of  $1 \times 10^{20} \text{ cm}^{-3}$  can exhibit a high PF of  $\sim 19 \mu\text{W cm}^{-1} \text{K}^{-2}$  and a peak  $zT$  of 1.7, resulting mainly from the increased density of states effective mass. Therefore, pressure tuning is an effective method to improve the p-type and n-type thermoelectric transport performance of  $\text{Mg}_3\text{Sb}_2$ -based Zintl compounds. This work

on  $\text{Mg}_3\text{Sb}_2$  under pressure may provide a new mechanism for experimenters to the enhancement of the thermoelectric performance of materials.

## Conflicts of interest

There are no conflicts to declare.

## References

- 1 L. E. Bell, *Science*, 2008, **321**, 1457–1461.
- 2 B. Jiang, Y. Yu, J. Cui, X. Liu, L. Xie, J. Liao, Q. Zhang, Y. Huang, S. Ning, B. Jia, B. Zhu, S. Bai, L. Chen, S. Pennycook and J. He, *Science*, 2021, **371**, 830–834.
- 3 J. Mao, H. Zhu, Z. Ding, Z. Liu, G. A. Gamage, G. Chen and Z. Ren, *Science*, 2019, **365**, 495–498.
- 4 S. Roychowdhury, T. Ghosh, R. Arora, M. Samanta, L. Xie, N. K. Singh, A. Soni, J. He, U. V. Waghmare and K. Biswas, *Science*, 2021, **371**, 722–727.
- 5 K. Imasato, C. Fu, Y. Pan, M. Wood, J. Kuo, C. Felser and G. J. Snyder, *Adv. Mater.*, 2020, **32**, 1908218.
- 6 K. Imasato, S. D. Kang, S. Ohno and G. J. Snyder, *Mater. Horiz.*, 2018, **5**, 59–64.
- 7 L. Zhao, G. Tan, S. Hao, J. He, Y. Pei, H. Chi, H. Wang, S. Gong, H. Xu, V. P. Dravid, C. Uher, G. J. Snyder, C. Wolverton and M. G. Kanatzidis, *Science*, 2016, **351**, 141–145.
- 8 C. Chang, D. Wang, D. He, W. He, F. Zhu, G. Wang, J. He and L. Zhao, *Adv. Energy Mater.*, 2019, **9**, 1901334.
- 9 Z. Bu, X. Zhang, B. Shan, J. Tang, H. Liu, Z. Chen, S. Lin, W. Li and Y. Pei, *Sci. Adv.*, 2021, **7**, eabf2738.
- 10 X. Chen, H. Wu, J. Cui, Y. Xiao, Y. Zhang, J. He, Y. Chen, J. Cao, W. Cai, S. J. Pennycook, Z. Liu, L. Zhao and J. Sui, *Nano Energy*, 2018, **52**, 246–255.
- 11 Q. Zhu, S. Song, H. Zhu and Z. Ren, *J. Power Sources*, 2019, **414**, 393–400.
- 12 J. Zhang, L. Song, G. K. H. Madsen, K. F. F. Fischer, W. Zhang, X. Shi and B. B. Iversen, *Nat. Commun.*, 2016, **7**, 10892.
- 13 J. Zhang, L. Song, S. H. Pedersen, H. Yin, L. T. Hung and B. B. Iversen, *Nat. Commun.*, 2017, **8**, 13901.
- 14 J. Zhang, L. Song, A. Mamakhel, M. R. V. Jørgensen and B. B. Iversen, *Chem. Mater.*, 2017, **29**, 5371–5383.
- 15 A. Bhardwaj, A. Rajput, A. K. Shukla, J. J. Pulikkotil, A. K. Srivastava, A. Dhar, G. Gupta, S. Auluck, D. K. Misra and R. C. Budhani, *RSC Adv.*, 2013, **3**, 8504.
- 16 C. L. Condrona, S. M. Kauzlarich, F. Gascoin and G. J. Snyder, *J. Solid State Chem.*, 2006, **179**, 2252–2257.
- 17 K. Imasato, S. D. Kang and G. J. Snyder, *Energy Environ. Sci.*, 2019, **12**, 965–971.
- 18 K. Imasato, S. Ohno, S. D. Kang and G. J. Snyder, *APL Mater.*, 2018, **6**, 016106–016111.
- 19 J. Li, S. Zhang, S. Zheng, Z. Zhang, B. Wang, L. Chen and G. Lu, *J. Phys. Chem. C*, 2019, **123**, 20781–20788.
- 20 S. Ohno, K. Imasato, S. Anand, H. Tamaki, S. D. Kang, P. Gorai, H. K. Sato, E. S. Toberer, T. Kanno and G. J. Snyder, *Joule*, 2018, **2**, 141–154.
- 21 Z. Ren, J. Shuai, J. Mao, Q. Zhu, S. Song, Y. Ni and S. Chen, *Acta Mater.*, 2018, **143**, 265–271.
- 22 X. Shi, X. Wang, W. Li and Y. Pei, *Small Methods*, 2018, **2**, 1800022.
- 23 L. Song, J. Zhang and B. B. Iversen, *J. Mater. Chem. A*, 2017, **5**, 4932–4939.
- 24 H. Tamaki, H. K. Sato and T. Kanno, *Adv. Mater.*, 2016, **28**, 10182–10187.
- 25 J. Li, F. Jia, S. Zhang, S. Zheng, B. Wang, L. Chen, G. Lu and L. Wu, *J. Mater. Chem. A*, 2019, **7**, 19316–19323.
- 26 J. Mao, J. Shuai, S. Song, Y. Wu, R. Dally, J. Zhou, Z. Liu, J. Sun, Q. Zhang, C. d. Cruz, S. Wilson, Y. Pei, D. J. Singh, G. Chen, C. W. Chu and Z. Ren, *Proc. Natl. Acad. Sci. U. S. A.*, 2017, **114**, 10548–10553.
- 27 X. Shi, T. Zhao, X. Zhang, C. Sun, Z. Chen, S. Lin, W. Li, H. Gu and Y. Pei, *Adv. Mater.*, 2019, **31**, 1903387.
- 28 J. F. Meng, D. A. Polvani, C. D. W. Jones, F. J. DiSalvo, Y. Fei and J. V. Badding, *Chem. Mater.*, 2000, **12**, 197–201.
- 29 S. D. Guo and J. L. Wang, *RSC Adv.*, 2016, **6**, 31272–31276.
- 30 L. Xu, Y. Zheng and J. C. Zheng, *Phys. Rev. B: Condens. Matter Mater. Phys.*, 2010, **82**, 195102.
- 31 Y. Zhang, S. Hao, L. D. Zhao, C. Wolverton and Z. Zeng, *J. Mater. Chem. A*, 2016, **4**, 12073–12079.
- 32 D. A. Polvani, J. F. Meng, N. V. C. Shekar, J. Sharp and J. V. Badding, *Chem. Mater.*, 2001, **13**, 2068–2071.
- 33 J. Li, S. Zhang, F. Jia, S. Zheng, X. Shi, D. Jiang, S. Wang, G. Lu, L. Wu and Z.-G. Chen, *Mater. Today Phys.*, 2020, **15**, 100269.
- 34 X. Tang, B. Zhang, X. Zhang, S. Wang, X. Lu, G. Han, G. Wang and X. Zhou, *ACS Appl. Mater. Interfaces*, 2020, **12**, 8359–8365.
- 35 J. Zhang, L. Song and B. B. Iversen, *ACS Appl. Mater. Interfaces*, 2021, **13**, 10964–10971.
- 36 P. E. Blöchl, *Phys. Rev. B: Condens. Matter Mater. Phys.*, 1994, **50**, 17953–17979.
- 37 G. Kresse and J. Hafner, *Phys. Rev. B: Condens. Matter Mater. Phys.*, 1993, **47**, 558–561.
- 38 G. Kresse and D. Joubert, *Phys. Rev. B: Condens. Matter Mater. Phys.*, 1999, **59**, 1758–1775.
- 39 J. Li, S. Zhang, B. Wang, S. Liu, L. Yue, G. Lu and S. Zheng, *J. Mater. Chem. A*, 2018, **6**, 20454–20462.
- 40 J. Li, S. Zheng, T. Fang, L. Yue, S. Zhang and G. Lu, *Phys. Chem. Chem. Phys.*, 2018, **20**, 7686–7693.
- 41 D. J. Singh, *Phys. Rev. B: Condens. Matter Mater. Phys.*, 2010, **82**, 205102.
- 42 F. Tran and P. Blaha, *Phys. Rev. Lett.*, 2009, **102**, 226401.
- 43 A. Fonari and C. Sutton, *Effective Mass Calculator*, 2012, <http://github.com/afonari/emc>.
- 44 G. K. H. Madsen, J. Carrete and M. J. Verstraete, *Comput. Phys. Commun.*, 2018, **231**, 140–145.
- 45 J. Bardeen and W. Shockley, *Phys. Rev.*, 1950, **80**, 72–80.
- 46 D. G. Cahill, S. K. Watson and R. O. Pohl, *Phys. Rev. B: Condens. Matter Mater. Phys.*, 1992, **46**, 6131–6140.
- 47 R. Santos, S. A. Yamini and S. X. Dou, *J. Mater. Chem. A*, 2018, **6**, 3328–3341.
- 48 T. Fang, S. Zheng, T. Zhou, L. Yan and P. Zhang, *Phys. Chem. Chem. Phys.*, 2017, **19**, 4411–4417.



- 49 M. Calderón-Cueva, W. Peng, S. M. Clarke, J. Ding, B. L. Brugman, G. Levental, A. Balodhi, M. Rylko, O. Delaire, J. P. S. Walsh, S. M. Dorfman and A. Zevalkink, *Chem. Mater.*, 2021, **33**, 567–573.
- 50 S. Ding, R. Su, W. Cui, J. Hao, J. Shi and Y. Li, *ACS Omega*, 2020, **5**, 31902–31907.
- 51 S. W. Song, J. Mao, M. Bordelon, R. He, Y. M. Wang, J. Shuai, J. Y. Sun, X. B. Lei, Z. S. Ren, S. Chen, S. Wilson, K. Nielsch, Q. Y. Zhang and Z. F. Ren, *Mater. Today Phys.*, 2019, **8**, 25–33.
- 52 J. Shuai, Y. Wang, H. S. Kim, Z. Liu, J. Sun, S. Chen, J. Sui and Z. Ren, *Acta Mater.*, 2015, **93**, 187–193.

